

# Imaging of Homeostatic, Neoplastic, and Injured Tissues by HA-Based Probes

Mandana Veiseh,<sup>†</sup> Daniel Breadner,<sup>‡</sup> Jenny Ma,<sup>‡,§,||</sup> Natalia Akentieva,<sup>‡,§,||</sup> Rashmin C Savani,<sup>¶</sup> Rene Harrison,<sup>†</sup> David Mikilus,<sup>▲</sup> Lisa Collis,<sup>□</sup> Stefan Gustafson,<sup>●</sup> Ting-Yim Lee,<sup>#,▽</sup> James Koropatnick,<sup>‡,§,▽,◆</sup> Leonard G. Luyt,<sup>‡,§,‡,▽</sup> Mina J. Bissell,<sup>†</sup> and Eva A. Turley<sup>\*,‡,§,||</sup>

<sup>†</sup>Division of Life Sciences, Lawrence Berkeley National Laboratories, Berkeley, California

<sup>‡</sup>Lawson Health Research Institute and London Regional Cancer Program, London Health Sciences Centre, Departments of <sup>§</sup>Oncology, <sup>||</sup>Biochemistry, <sup>‡</sup>Chemistry, <sup>#</sup>Medical Biophysics, <sup>▽</sup>Medical Imaging, Microbiology and Immunology, <sup>○</sup>Physiology and Pharmacology and <sup>◆</sup>Pathology, The University of Western Ontario, London, Canada

<sup>¶</sup>Department of Pediatrics, University of Texas Southwestern Medical School, Dallas, Texas

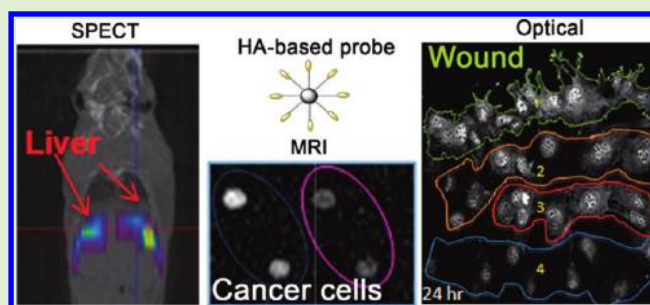
<sup>†</sup>Department of Biological Sciences, University of Toronto at Scarborough, Toronto, Canada

<sup>▲</sup>Department of Medical Imaging, Institute of Medical Science, University of Toronto, Toronto, Canada

<sup>□</sup>Division of Cardiovascular Research, Hospital for Sick Children, Toronto, Canada

<sup>●</sup>Department of Medical and Physiological Chemistry, University of Uppsala, Uppsala, Sweden

**ABSTRACT:** An increase in hyaluronan (HA) synthesis, cellular uptake, and metabolism occurs during the remodeling of tissue microenvironments following injury and during disease processes such as cancer. We hypothesized that multimodality HA-based probes selectively target and detectably accumulate at sites of high HA metabolism, thus providing a flexible imaging strategy for monitoring disease and repair processes. Kinetic analyses confirmed favorable available serum levels of the probe following intravenous (i.v.) or subcutaneous (s.c.) injection. Nuclear (technetium-HA, <sup>99m</sup>Tc-HA, and iodine-HA, <sup>125</sup>I-HA), optical (fluorescent Texas Red-HA, TR-HA), and magnetic resonance (gadolinium-HA, Gd-HA) probes imaged liver (<sup>99m</sup>Tc-HA), breast cancer cells/xenografts (TR-HA, Gd-HA), and vascular injury (<sup>125</sup>I-HA, TR-HA). Targeting of HA probes to these sites appeared to result from selective HA receptor-dependent localization. Our results suggest that HA-based probes, which do not require polysaccharide backbone modification to achieve favorable half-life and distribution, can detect elevated HA metabolism in homeostatic, injured, and diseased tissues.



## INTRODUCTION

Tissue microenvironments undergo remarkably similar remodeling events during normal response-to-injury and disease processes (e.g., cancer). One remodeling process that is common to both tissue repair and disease processes is the increased metabolism of the extracellular polysaccharide hyaluronan (HA). Increased metabolism of HA is an early, tightly regulated, and transient remodeling event in most normal response-to-injury processes<sup>1–3</sup> and is constitutively active in many cancers. When robust repair results from procedures such as balloon angioplasty of coronary arteries (a process termed restenosis)<sup>4,5</sup> or in injury-sensitive organs such as the brain (e.g., repair resulting from stroke),<sup>6</sup> the normal tissue injury/repair process can have adverse clinical effects. The development of imaging probes able to track the course of repair and cancer progression would greatly aid treatment and outcome, particularly when probes are flexible

enough to allow detection of disease in multiple modalities because each imaging method has unique advantages.

Native HA is a large, linear, and negatively charged glycosaminoglycan that is present in small amounts in most homeostatic adult tissues. It performs scaffolding functions and contributes to sustaining normal tissue architecture. In normal physiology, the liver, kidney, and lymphatic systems participate in the turnover and removal of excess tissue HA.<sup>7–11</sup> It is removed from serum by endocytic HA receptors in the liver and, to a lesser extent, by the kidneys. Injury-induced HA metabolism differs substantially from the homeostatic turnover of HA. Elevated HA levels in injured tissues result from the increased expression/activation of HA synthases (HAS1–3). Newly synthesized HA is fragmented locally by release of

Received: April 6, 2011

Revised: October 18, 2011

Published: November 9, 2011

hyaluronidases (e.g., HYAL-1, 2), and formation of reactive oxygen species (ROS). Tissue injury induces the expression/activation of HA receptors such as Cluster Designation 44 (CD44), receptor for HA-mediated motility (RHAMM/HMMR), and Toll-like receptors 2, 4 (TLR2, 4), which bind to these HA fragments.<sup>2,3,12,13</sup> Fragmented HA:HA receptor interactions activate signaling cascades required for migration/proliferation/differentiation of incoming somatic and immune cells. The signaling function of HA fragments is terminated by their cellular uptake via HA receptor-mediated endocytosis.

Elevated HA metabolism that resembles this injury response also occurs constitutively in some types of human cancers and has been linked to tumor aggression and progression.<sup>14–16</sup> For example, increased deposition of HA and increased expression of the HA receptors, CD44 and RHAMM, are prognostic indicators of poor outcome in breast cancer. HA accumulation is chronically elevated in neoplastic breast versus normal tissue primarily as a result of increased HAS expression. Constitutive, localized HA fragmentation results from elevated expression/release of hyaluronidases and ROS formation. As for tissue injury responses, these activate signaling cascades through CD44/RHAMM/TLR2, 4 to promote tumor and macrophage/stromal cell migration and survival.<sup>8,16–18</sup>

The HA polymer is amenable to chemical modification, and some of these modified forms are currently used clinically as components of engineered tissues and grafts.<sup>19–21</sup> Other forms are in preclinical assessment for enhancing targeting/efficacy of some classes of drugs (e.g., topical application of small molecules<sup>22</sup>) and, to a lesser extent, for use in imaging.<sup>23–25</sup> Recently, we showed that intravenous (i.v.) infusion of 1.5–12 mg/kg into healthy human subjects unexpectedly revealed that HA has a prolonged serum half-life (i.e., an administered dose of 3 mg/kg has a  $T_{1/2} = 12$  h) and impressive safety profile.<sup>26</sup> These results favor clinical development of an unmodified HA polymer as an imaging probe that can be delivered intravenously. Here we analyzed kinetic properties of HA-based probes following i.v., s.c., and oral administration and evaluated their targeting ability to homeostatic, neoplastic, and injured tissues in both culture and animal models. We developed a set of HA-based probes that carried nuclear, fluorescence, or magnetic resonance contrast agents on a native HA polymer backbone. To test the targeting properties of these probes, we chose liver as a model of a homeostatic tissue with high HA metabolism, MDA-MB-231, and MCF-7 cell lines/xenografts as models of aggressive versus less aggressive breast cancer<sup>27</sup> and a balloon-injured carotid artery as an example of a vascular response-to injury.

## ■ EXPERIMENTAL SECTION

**Measurement and Detection of HA Levels.** To quantify serum and tissue HA, the HA-binding region of aggrecan (HABP) was isolated, purified from bovine nasal cartilage as previously described,<sup>28</sup> and then biotinylated. HA levels in carotid arteries and serum were measured using HRP-conjugated avidin in an ELISA assay and then stained with diaminobenzidine.<sup>29</sup> Organs including both injured and uninjured carotid arteries were harvested, rinsed in PBS, and weighed. Tissue components were isolated as previously described.<sup>30</sup> Total protein was determined using a BioRad protein determination kit.

**Kinetic Analyses.** Kinetic analysis of HA absorption and elimination following i.v., s.c., or oral administration was performed in Sprague–Dawley rats (female, 3 month old, average weight = 250 g,  $n = 5$  rats) using data obtained from 0.3 mL of blood drawn from rat tail veins at indicated times of between 0 and 96 h after a single dose of

HA. The sera from blood samples were obtained by centrifugation and immediately frozen and stored at  $-20$  °C for later HA analysis.

**Molecular Weight Analyses of Serum HA.** For molecular weight analysis, HA was precipitated from serum, as previously described.<sup>31</sup> Serum fractions and dextran blue molecular weight standards were applied to a Sephadex G-100 column, 0.5 mL fractions were collected, and amounts of HA present in each fraction were determined by ELISA as above. The void volume of columns was established using dextran blue ( $10^6$  Da), and the included volume was determined using methylene blue dye (200 Da). Dextran blue polymers of varying sizes (50–400 kDa) were used as reference standards. HA present in the fractionated serum was detected using the above ELISA. The molecular weight range of the HA used for the experiments (50–500 kDa with a peak at 240 kDa) was also assessed using this method (data not shown).

**Preparation of HA-Based Imaging Probe. Labeling of HA with  $^{99m}\text{Tc}$ .** The labeling of HA was conducted using a procedure modified from Balogh et al.<sup>32</sup> We added 0.1 mL of aqueous stannic chloride (2 mg/mL) to 9 mg of HA in 0.1 mL of a 0.1 M NaOAc solution, followed by the addition of 0.2 mL of 0.1 M sodium D-gluconate prior to the addition of aqueous  $^{99m}\text{TcO}_4$  (30 mCi in 0.5 mL). The solution was stirred at 60 °C for 60 min. The reaction mixture was eluted on a column of Sephadex G-50 (fine) to remove the unincorporated radioisotope, stannic chloride, and D-gluconate.  $\text{H}_2\text{O}$  was removed in vacuo, providing  $^{99m}\text{Tc}$ -labeled HA.

**Labeling of HA with  $^{125}\text{I}$ .** Medical-grade HA was supplied by Hyal Pharmaceutical (Mississauga, Ontario). The molecular weight distribution of HA was established by gel filtration as described<sup>26</sup> previously and estimated to be 240 kDa. HA was labeled with DL-tyrosine (Sigma) as previously described<sup>33</sup> after cyanogen bromide (CNBr) activation of the polysaccharide. In brief, 15 mg of HA or chondroitin sulfate (CS) were activated at a pH of 11 with 8 mg CNBr for 5 min. The activated polysaccharide was separated from the reaction mixture on a desalting, Sephadex G-25 column (Pharmacia) equilibrated with 0.2 M borate buffer (pH 8.0). The activated polysaccharide was incubated overnight with 1 mg tyrosinase (Sigma). T-bound HA (T-HA) was separated from unbound T on a Sephadex G-25 column equilibrated with phosphate-buffered saline (pH 7.5). T-HA (100  $\mu\text{g}$ ) was iodinated with  $^{125}\text{I}$  by incubating it with 0.5 mCi  $^{125}\text{I}$  in a glass container and covering the solution with a film of 10  $\mu\text{g}$  1,3,4,6-tetrachloro-6-sulpho-diphenylglycouril (Sigma Chemicals). Unreacted  $^{125}\text{I}$  was removed by separation on a Sephadex G-25 column equilibrated with PBS, as described above.  $^{125}\text{I}$ -HA (specific activity 1500–5000 dpm/ng) maintained its high-molecular-weight profile and was stored at 4 °C.

**Labeling of HA with Texas Red (TR).** To study HA uptake into human breast cancer cell lines, cells were exposed to 0.01 to 1.0 mg/mL HA that was conjugated to TR hydrazide through 1-ethyl-3-dimethylaminopropyl carbodiimide (EDC) coupling reagent (Sigma). The TR hydrazide concentration was titrated to achieve a theoretical decoration of HA with 1 TR molecule per 10 HA residues.

**Labeling of HA with Gd.** Diethylenetriaminepentaacetic acid (DTPA) was conjugated to HA as previously described.<sup>34</sup> The level of conjugation was measured by isothermal titration calorimetry (ITC) and colorimetry, which provides more accurate quantification than  $^1\text{H}$  NMR spectroscopy due to differences in proton relaxation times in HA-DTPA polymer backbone versus freely DTPA side chain.<sup>34</sup> In brief, HA was first reacted with ethylenediamine in the presence of EDC (Sigma Chemicals), which was used as a coupling agent in a 2-(*N*-morpholino) ethanesulfonic acid<sup>5</sup> buffer (pH 4.5). The ethylenediamine-modified HA was then purified by dialysis and reacted with DTPA activated in a separate reaction with a dicyclohexylcarbodiimide/*N*-hydroxy-sulfosuccinimide mixture in dimethyl sulfoxide (DMSO). The product, HA-DTPA, was purified by three separate filtration steps using membranes with a molecular cutoff of 3500 Da. An absence of free DTPA was confirmed by analysis with an arsenazo test and gravimetry.<sup>34</sup> Both techniques indicated a recovery of 97% HA-DTPA.  $\text{GdCl}_3 \cdot 6\text{H}_2\text{O}$  (4–7 mg) (Sigma Chemicals) was added to 13 mL of HA-DTPA (1.5 mg/mL) and filtered using YM-10 membranes (MW cutoff, 10 kDa). The concentrated polymer solution

was washed four times with water, and  $Gd^{3+}$  was monitored in the filtrate. All excess, unbound  $Gd^{3+}$  was detected in the first three washes. The DTPA content in the end product was measured by isothermal calorimetry and a colorimetric assay. One gadolinium ion ( $Gd^{3+}$ ) bound to 1 DTPA unit and both techniques gave a similar DTPA content of 0.32 mmol DTPA/g polymer with 15.0 mol % of the carboxylic acid groups of HA bearing a DTPA unit. T1 values of HA-DTPA-GD were measured in deionized water at 25 °C, as described.<sup>35</sup> The R1 relaxivity of the product was measured as 6 nmol/L/s per Gd, and the R2 relaxivity was measured as 12 nmol/L/s per Gd and is similar to previous reports.<sup>35,36</sup>

**Single-Photon Emission Computed Tomography/Computed Tomography (SPECT/CT) Imaging of Mice Injected with <sup>99m</sup>Tc-Labeled HA.** C57/BL6 mice were purchased from Charles River (3 month old females, average weight = 22 g,  $n = 5$ /treatment). The labeled HA was dissolved in a sterile saline solution and drawn into 0.2 mL doses (1.2 mCi) for tail-vein injection. All CS doses were 5 mg in 0.15 mL of sterile saline. Three cohorts were used: five mice received only the labeled HA; five mice received an i.v. CS dose, followed immediately by the labeled HA; and five mice received an i.v. CS, followed by an i.p. dose, immediately followed by the labeled HA. Animals were anesthetized during imaging: animals were anesthetized with 3% isoflurane with oxygen in a chamber to start, then with 2% isoflurane for tail vein catheterization and isotope injection. During SPECT/CT imaging, mice were anesthetized with 3% isoflurane with oxygen in a chamber, then with 1.5% isoflurane through a mask while on the imaging bed. All mice were imaged at 120 min and euthanized at 150 min. The animals were dissected, and specific organs or tissues were removed for biodistribution studies. All SPECT/CT scans were performed using the eXplore speCZT for small animal imaging (GE Healthcare). Transaxial and axial resolution were 1.2 and 1.6 mm respectively, with a total scan time of 26 min per scan.

**Breast Tumor Cell Culture.** MDA-MB-231 and MCF-7 cells were purchased from ATCC (MDA-MB-231, HTB-26, MCF7, HTB-22). Cells were maintained under routine 2-D culture conditions (passaged 1:4 at confluence, DMEM + 10% fetal bovine serum, 37 °C and 5%  $CO_2$ ). Three-dimensional cultures of MDA-MB-231 and MCF-7 human breast cancer cell lines were prepared by forming aggregates from freshly trypsinized cells by shaking on a nutator set at 50 rpm in a humidified atmosphere containing 5%  $CO_2$  at 37 °C for 4–6 h. Aggregates were recovered by centrifugation and embedded within Bovine type I collagen (BD Biosciences) prepared as per the manufacturer's instructions.

**Flow Cytometry.** MDA-MB-231 breast tumor cells were plated at a density of 50% in T75 plastic tissue culture flask in DMEM + 10% FBS and then rinsed with  $Ca^{2+}$ -free Hanks balanced salt solution (HBSS) supplemented with 20 mM Hepes. Cells were removed from the flask surface using nonenzymatic dissociation medium (Sigma), centrifuged, resuspended in cold phosphate-buffered saline, and blocked in cold 10% FBS/HBSS/HEPES buffer<sup>27</sup> for 1 h at 4 °C. The viability of harvested cells was checked using a Vi-CELL cell viability analyzer and was confirmed to be 85–95% (2.5 million/ml cells were used for analysis). Cell surface CD44 was detected using IM-7 monoclonal antibody (Pharmingen, 7.5  $\mu$ g/mL in PBS/BSA, 2%) for 45 min at 4 °C. The CD44 antibody was directly conjugated to Alexa Fluor 647 (Invitrogen) prior to sample preparation. Cells were washed with 2% PBS/BSA two times, and living cells were analyzed using a BD FACS flow cytometer (BD Biosciences). MCF-7 cells were prepared in the same manner but were also resuspended in DMEM phenol-free medium (Invitrogen) to enhance viability. Data analysis was performed using Flow Jo software.

**Addition of TR-HA to Breast Cancer Cell Lines.** TR-HA and FITC-dextran (10 000 Da, Sigma) were added for 10–30 min to subconfluent (50%), adherent cells that had previously been subcultured onto glass coverslips for 12 h. To block the HA binding function of CD44 in breast cancer cell lines, 50  $\mu$ g/mL anti-CD44 antibody (clone KM201, R&D Systems) was added to live cells for 5 min, as per manufacturer's instructions, prior to the addition of TR-HA. Cells were then fixed in 3% paraformaldehyde containing 1% cetylpyridinium chloride (Sigma) to precipitate glycosaminoglycans.

FITC-dextran was used as a marker for general uptake of polysaccharides. Coverslips were mounted onto glass slides and examined using a Zeiss Axio Imager A1 microscope. The amount of TR and FITC-dextran uptake was quantified using Elements 3 image analysis software, and the results were used to calculate the ratio of TR uptake to FITC-dextran uptake.

**Xenograft Formation and MRI.** MDA-MB-231 cells or MCF-7 cells ( $1 \times 10^6$  cells/injection site) were suspended in matrigel and were injected into the flanks of nude rats (Charles River, 3 month old females, average weight = 250 g,  $n = 5$  animals) and grown for ~3 weeks to 1 cm<sup>3</sup>. Tumor-bearing animals were sedated to reduce artifacts due to motion as above, injected intravenously with Gd-HA (0.1–10 mg/kg, 1 mg/kg shown in this study to be optimal dose),<sup>35</sup> and imaged using a 0.3T permanent magnet MR AIRIS (open type Hitachi Medico) as described.<sup>36</sup> The xenografts were imaged over a time frame of 5 min to 2 h. Because maximal signal was obtained between 20 min and 2 h, animals were imaged for 20 min after i.v. injection of the Gd-HA probe.

**Wound Assays.** C3H/10T1/2 fibroblasts were purchased from ATCC (CCL-226, clone 8). Confluent 10T1/2 fibroblast monolayers growing in DMEM supplemented with 10% fetal bovine serum (Intergeren) were scratch-wounded with a plastic 500  $\mu$ L pipet tip, washed to remove detached cells, and incubated in fresh DMEM + 10% FCS for 24 h. Injured cultures were then exposed to TR-HA probe (0.1–100  $\mu$ g) for 10 min. Cells were rinsed in cold PBS to prevent release of bound TR HA probe during washing<sup>37,38</sup> and fixed in a solution of freshly prepared 3% paraformaldehyde and 1% cetylpyridinium chloride in a 0.1 N Na-phosphate buffer (pH 7.4) for 10 min at 25 °C. Coverslips were washed three times in PBS, mounted with elvanol, and viewed using a Zeiss confocal microscope.

**Serum Starvation Assays.** Smooth muscle cells were isolated from rat aorta,<sup>39</sup> and the endothelial layer was stripped using sterile forceps. Strips of the exposed medial layer of the vessel were then cut into 1 mm<sup>3</sup> pieces and cultured in DMEM (GIBCO BRL) supplemented with 10% FBS, 20 mM Hepes buffer (pH 7.2), and 1% penicillin/streptomycin mixture. Smooth muscle cells that migrated out of the explants were subcultured and maintained in DMEM supplemented with 10% FCS at 37 °C and 5%  $CO_2$ . Only cells of low passage number (<10) were used for further study. Serum starvation was performed in defined DMEM medium (0.5 U/mL insulin and 4  $\mu$ g/mL transferrin) for 48 h, and then defined medium was replaced with DMEM containing 10% fetal bovine serum.<sup>40</sup> Cells were exposed to serum supplements for 24 h, followed by addition of TR-HA as described above, and cultures were processed/photographed as described for fibroblasts.

**Balloon Injury of Rat Carotid Arteries.** Sprague Dawley rats were purchased from Charles River (3 month old females, average weight = 225 g,  $n = 4$  animals). All animal procedures were done in conformity with the animal use practices at the University of Toronto. The procedure was performed as described.<sup>41</sup> The truncation point of the common to external and internal carotid arteries was located and isolated, and the common and internal branches were clamped. The external branch was sutured as distal to the truncation as possible, and a Fogarty 2F balloon catheter was inserted into an incision made in the external branch and fed through to the common carotid artery. The endothelium within the common carotid was removed (denudation) in ~1.5 cm of its length, by four draws of a balloon catheter within 20 s at an estimated pressure of 3.0 atm. After this injury, the catheter was removed, and the external branch was sutured on the other side of the incision.

**Measurement of Myeloperoxidase and Glucosaminidase.** Myeloperoxidase (MPO) activity (a marker for activated neutrophils) was measured in protein extracts of carotid arteries using the EnzChek MPO assay kit (Invitrogen) according to the manufacturer's instructions. Glucosaminidase activity was assayed as previously described.<sup>42</sup>

**Western Immunoblots.** Cell lysates were prepared from monolayers grown to 50% density on plastic tissue culture plates, and proteins were separated by SDS-PAGE. Immunoblot analysis of CD44 and RHAMM proteins was conducted as previously described.<sup>27</sup>

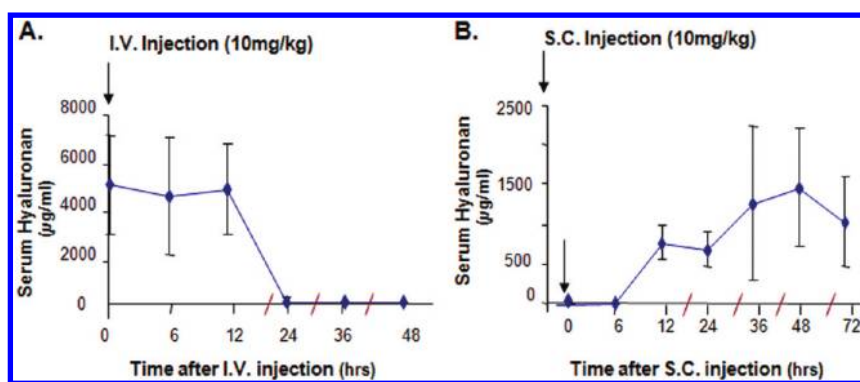


**Figure 1.** Serum levels of HA after i.v. and s.c. injection. (A) Serum HA levels are sustained for ~12 h after i.v. injection and fall to baseline level over time following i.v. injection (10 mg/kg) in rats. (B) Serum HA levels gradually increase over time following s.c. injection (10 mg/kg) in the flank of rats. Levels of serum HA initially increase above baseline levels by exogenous HA injected by i.v. and s.c. All values indicate mean and SEM ( $n = 2$  samples from each of five rats).

**Administration of  $^{125}\text{I}$  and Unlabeled HA.** Male Sprague–Dawley rats (370–460 g) were anesthetized by s.c. injection with ketamine (80 mg/kg), xylazine (40 mg/kg), and atropine (0.05 mg/kg).  $^{125}\text{I}$  HA (1.2–5 mg) or unlabeled HA (3–10 mg/kg) was injected in a 0.8 to 1.0 bolus into the penile vein 2–24 h after the carotid artery was injured by balloon catheter, as described above. An i.v. bolus of unlabeled HA was administered every day over 5 days to analyze its effects on white cell infiltration and neointima formation. To assess the effect of treatment with exogenous HA, HA (10 mg/kg in 1.0 to 2.0 mL PBS) was injected under the skin of the right flank immediately postoperation and again at 48 and 96 h postoperation. HA was administered by oral gavage (3.0–10 mg/kg every 3 days, between 9 and 10 a.m.). An animal feeding needle of 18Qx2 was used for gavage.

**Scintigraphic Studies.** At 2–24 h after injection of rats with  $^{125}\text{I}$ -HA and injury of carotid artery, rats were euthanized, and both carotid arteries were removed and snap frozen. Cryosections (50  $\mu\text{m}$ ) were prepared and placed adjacent to a CS-screen to capture the  $^{125}\text{I}$  signal. After 7 days, the screen was developed and analyzed on a Bio-Rad GS-525 phosphorimager with Molecular Analyst software (Molecular Dynamics). Statistical analyses were performed using Statworks.

## RESULTS

**Kinetic Properties of HA Administered via Different Routes.** We have reported that increasing the concentration of i.v. injected HA (e.g., 1.5–12 mg/kg also) can safely increase serum half-life from minutes to >12 h in healthy human subjects.<sup>26</sup> To characterize the serum half life in rats and to identify the optimal route of administration for HA-based probe targeting, we compared the kinetic parameters of serum HA after i.v., s.c., and oral administration (3–10 mg/kg HA, 10 mg/kg shown, Figure 1, Table 1) in rats. Following i.v. injection, serum HA levels reached 5000  $\mu\text{g}/\text{mL}$ , remained high

**Table 1.** Pharmacokinetic Parameters of HA in Serum<sup>a</sup>

route of administration	$C_{\text{max}}$ (ug/mL) <sup>b</sup>	$T_{\text{max}}$ h <sup>c</sup>	AUC@72 h <sup>d</sup>	$F^e$
intravenous	5096.00	0–12	0	1.00
subcutaneous	1454.00	36–48	72	0.79
oral	0.15	12–36	6.01	0.0001

<sup>a</sup>Serum HA levels were measured using a competitive binding ELISA. Assays were done in triplicate, and background serum levels of HA were subtracted from experimental levels. Values used for kinetic analyses are from one experimental series. Animals were administered 10 mg/kg HA via i.v., s.c., or oral routes. <sup>b</sup> $C_{\text{max}}$  = maximum concentration achieved. <sup>c</sup> $T_{\text{max}}$  = time after administration when maximum concentration was achieved. <sup>d</sup>AUC = area under the curve. <sup>e</sup>F = absorption rate constant.

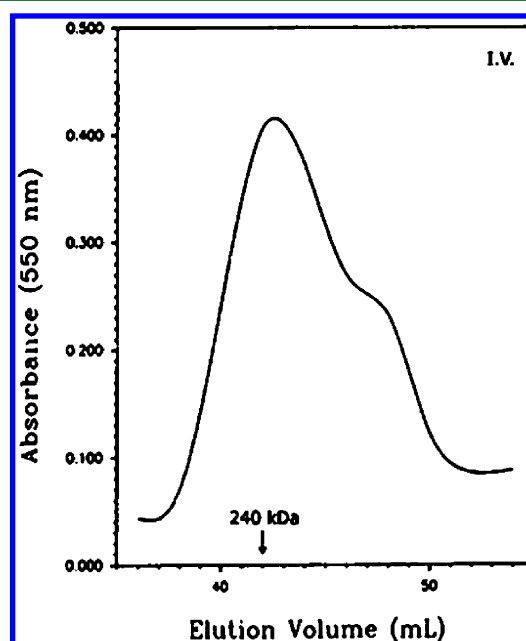


**Figure 2.** Molecular weight of serum HA is not detectably modified after i.v. injection. Gel filtration of serum HA was determined at  $C_{\text{max}}$  following injection by i.v. The  $MW_{\text{av}}$  of HA injected into animals was originally 240 kDa, and this size changes very slightly following i.v. injection (shoulder to the right). Scan shown here is from individual samples and is representative of scans obtained from five separate animals.

for a period of 12–24 h, and then decreased to the baseline levels (~75 ng/mL) (Figure 1A). A single s.c. injection of HA resulted in a gradual increase in serum HA levels over 24 h, reaching maximum levels of 1200  $\mu\text{g}/\text{mL}$  between 24 and 72 h postinjection (Figure 1B). Oral administration of HA caused small but significant increases in serum HA over baseline (110–145 ng/mL range,  $p < 0.01$ , data not shown). These low levels are in agreement with previous reports.<sup>43–46</sup> Kinetic analyses showed that the  $C_{\text{max}}$  of i.v. injected HA (10 mg/kg) was approximately 4 times and 34 000 times higher than the  $C_{\text{max}}$  of s.c. injected and oral gavage HA, respectively (Table 1). The fraction of HA absorbed into serum following s.c. injection was calculated to be 79% of i.v. administered HA, assuming an absorption of 100% following i.v. injection. Much less HA was systemically absorbed (0.01%) after oral gavage (Table 1).

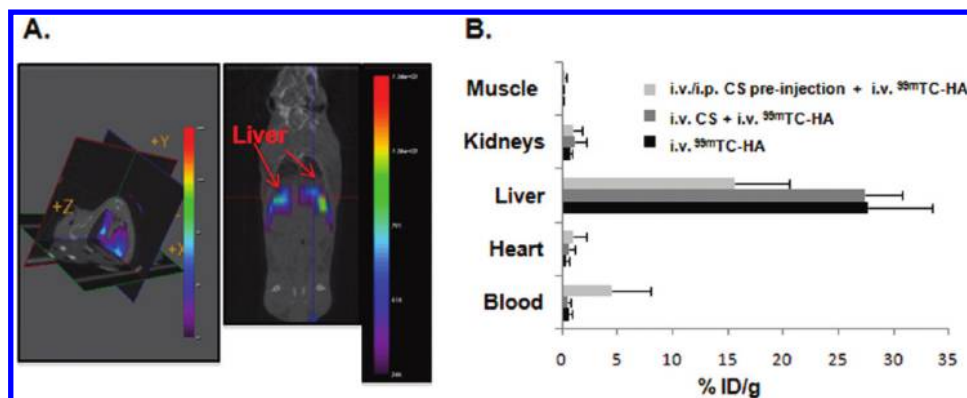


**Figure 3.**  $^{99m}\text{Tc}$ -HA localizes in liver via receptor-mediated targeting. (A) SPECT imaging of  $^{99m}\text{Tc}$ -HA (in two views) injected via i.v. route. The liver is the predominant organ that takes up the HA probe. (B) Biodistribution of HA probe confirms that the majority of label targets to the liver and i.v./i.p. administered CS, which also binds to liver HA receptors and has been given via a route reported to down-regulate these receptors,<sup>49</sup> significantly reduces liver uptake of HA probe: as reported, CS administered by i.v., which is a method that does not influence liver HA receptor display, had no noticeable effect on the biodistribution of the HA probe. Values are the mean and SEM  $n = 5$  animals.

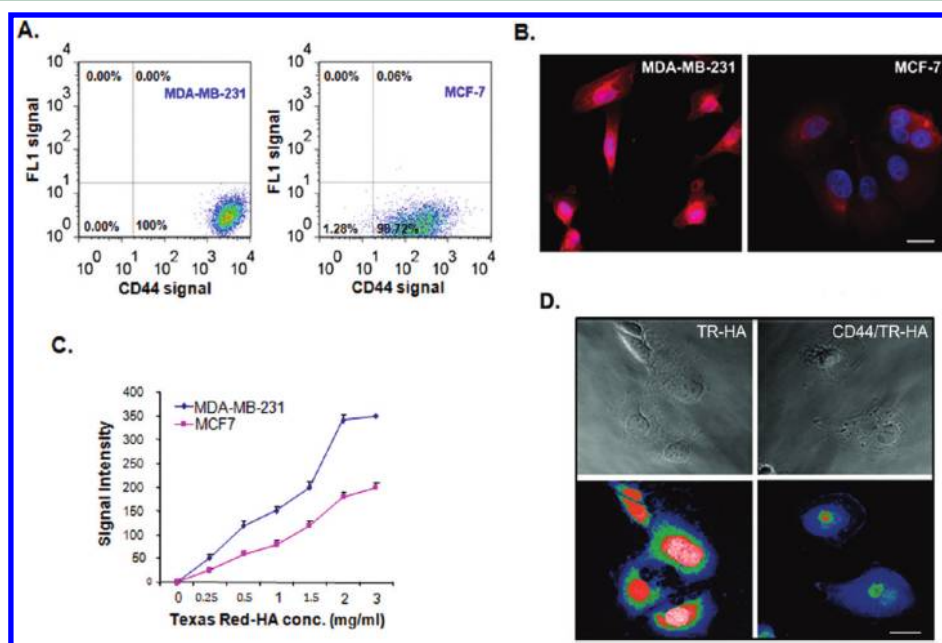


**Figure 4.** TR-HA and Gd-HA localized at a greater extent in aggressive MDA-MB-231 breast cancer cell compared with the less aggressive MCF-7.<sup>47</sup> (A) Flow cytometry analyses indicate that CD44 expression is higher in MDA-MB-231 than in MCF7 cells. (B,C) MDA-MB-231 cells take up TR-HA to a greater degree than MCF-7 breast cancer cells, correlating with CD44 surface display. (D) Uptake of TR-HA by MDA-MB-231 is inhibited by anti-CD44 antibodies. (scale bar = 10  $\mu\text{m}$ )

Because the size of the HA polymer may affect its targeting properties, we also analyzed the molecular weight distribution of serum HA following i.v. and s.c. injections as well as oral gavage, sampling close to the  $C_{\text{max}}$  (Figure 2). The initial  $MW_{\text{av}}$  of HA was 240 kDa.<sup>40</sup>

Gel filtration profiles showed that the majority of HA administered by either i.v. or s.c. injection eluted as high-molecular-weight polymers (Figure 2, i.v. injected profile shown). However, after oral administration,  $\sim 50\%$  of serum HA appeared as smaller fragments (data not shown), possibly resulting from fragmentation in tissues/lymphatics prior to its entering the blood vasculature.<sup>2,12</sup>

**HA Probes Target Liver through a Homeostatic Receptor-Mediated Process.** Liver is the predominant organ that takes up HA from serum during homeostasis. Therefore, we chose this organ to initially evaluate targeting ability of HA-based probes and to verify if uptake of our probe

occurs through a receptor-mediated endocytosis.<sup>7,48</sup> We prepared a sensitive  $^{99m}\text{Tc}$ -HA probe and followed its tissue distribution after i.v. injection of 1.2 mCi  $^{99m}\text{Tc}$ -HA (Figure 3A). Because no modifications were made to the HA used for radiolabeling, and because unreacted  $^{99m}\text{Tc}$  was removed during the  $^{99m}\text{Tc}$ -HA synthesis, one can reasonably assume that the  $^{99m}\text{Tc}$ -HA is behaving as per native HA, especially because there is at most one  $^{99m}\text{Tc}$  atom per HA molecule. As expected, the majority of injected  $^{99m}\text{Tc}$ -HA accumulated within the liver with an uptake value of 27.6% ID/g at 2.5 h postinjection (Figure 3A,B). Less than 5% of  $^{99m}\text{Tc}$ -HA uptake accumulated within the stomach and thyroid, which are the sites of uptake of free  $^{99m}\text{Tc}$  (data not shown).

Approximately 2% ID/g uptake of free  $^{99m}\text{Tc}$  was previously reported to accumulate within the liver.<sup>32</sup> To confirm that the accumulation of  $^{99m}\text{Tc}$ -HA in liver resulted from a receptor-mediated endocytosis rather than nonspecific uptake by

reticular endothelium, we blocked liver HA receptors by i.v. and i.p. preinjection of CS.<sup>49</sup> To control for potential chemical effects of CS on probe activity, we also injected this sulfated glycosaminoglycan at the same time as <sup>99m</sup>Tc-HA (referred to as i.v. CS + i.v. <sup>99m</sup>Tc-HA), a condition that does not result in down-regulation of liver HA receptors.<sup>50</sup> The i.v. injected CS + i.v. <sup>99m</sup>Tc-HA had little effect on the biodistribution of <sup>99m</sup>Tc-HA, whereas the combined i.v./i.p. preinjection of CS (referred to as i.v./i.p. CS preinjection + i.v. <sup>99m</sup>Tc-HA) significantly reduced <sup>99m</sup>Tc-HA liver uptake by 43% ( $p < 0.001$ , Figure 3). Blood levels of HA were correspondingly increased, consistent with inhibiting liver uptake of circulating <sup>99m</sup>Tc-HA probe. These results suggest that <sup>99m</sup>Tc-HA targets homeostatic liver via a receptor-mediated process in agreement with previous reports for <sup>125</sup>I-HA and quantum dot-HA.<sup>16,17,37,38,43,51,52</sup>

**TR-HA and Gd-HA Preferentially Target Aggressive Breast Cancer Cell Lines and Tumor Xenografts, Which Express High Levels of CD44.** Elevated expression of HA receptors such as CD44 and RHAMM are common in cancers and have been linked in some types of tumors to aggressive progression. HA-based imaging agents and therapeutics have previously been reported to effectively target tumors that express high levels of CD44.<sup>25,53–55</sup> We assessed if breast cancer cell lines that differed in CD44 expression level and degree of aggressiveness when grown in 3D culture or as xenografts could be identified by differential uptake of HA-based probes. To obtain accurate quantification at single cell, cellular aggregate, and tumor levels, we choose fluorescence and MRI as imaging modalities. The former provides superb 2-D lateral resolution, and the latter is widely used in the clinic for revealing anatomical details in 3-D soft tissues. We used MDA-MB-231 cells as an example of a breast cancer cell line, which displays high levels of CD44 and is aggressively tumorigenic, and MCF-7 cells, as an example of a less aggressive breast cancer cell line, which display lower levels of CD44.<sup>27,56,57</sup> Flow cytometry analysis confirmed that MDA-MB-231 cells displayed higher levels of cell-surface CD44 (geometric mean: 3009.88 for 100% of cells) compared with MCF-7 cells (geometric mean: 194.39 for 98.72% of cells) (Figure 4A), and fluorescence microscopy showed that MDA-MB-231 cells also took up more TR-HA than MCF-7 cells (Figure 4B,C), in agreement with the difference in surface display of CD44. The uptake of TR-HA into MDA-MB-231 cells was blocked by the KM201 anti-CD44 Mab (Figure 4D), directly demonstrating the role of CD44 as an endocytic HA receptor in this breast cancer cell line. We next designed a Gd-HA probe suitable for MRI imaging and assessed its ability to target MDA-MB-231 and MCF-7 cells and tumor xenografts (Figure 5). To define basal levels of Gd-HA uptake before xenografting, MDA-MB-231 and MCF7 cells were cultured as aggregates in 3D collagen gels, and their Gd-HA uptake was compared. As shown for TR-HA uptake (Figure 4C), Gd-HA probe uptake increased in a linear manner between 0.3 and 3.0 mg/mL (data not shown). MDA-MB-231 and MCF-7 xenografts were then grown on the flanks of nude rats for ease of detection. The HA probe was injected i.v., as previously reported for reagents that block CD44 function.<sup>58</sup> MRI images showed that Gd-HA, like TR-HA, was taken up to a greater extent in MDA-MB-231 than in MCF-7 cells (Figure 5A). Maximal probe uptake was observed at a concentration of 1 mg/kg. Gd-HA signal was clearly visible as early as 5–10 min after injection and a strong signal was observed at 20 min (Figure 5 B,C), which was preserved for 1–2 h (data not

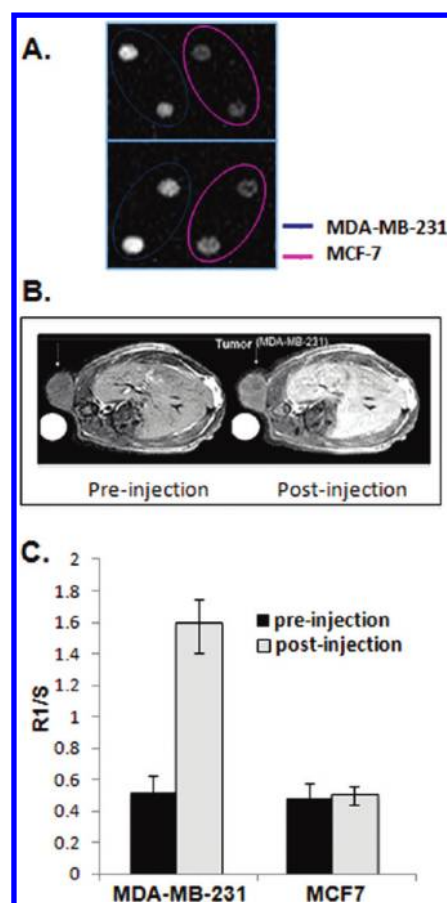


**Figure 5.** Gd-HA localized at a greater extent in 3D aggregates and tumor xenografts of MDA-MB-231 compared with MCF-7. (A) MDA-MB-231 cells take up Gd-HA to a greater degree than MCF-7 cells when grown as aggregates in 3D collagen gels. (B) MDA-MB-231 cell line, grown as a tumor xenograft, exhibits detectable levels of Gd-HA localized within the tumor mass (arrow). MRI is particularly well-suited for accomplishing this goal because optical sectioning allows simultaneous observation of weak and strong signals of different tissues in the same section. (C) MDA-MB-231 xenografts accumulate greater amounts of Gd-HA than MCF-7 xenografts.

shown). As shown in Figure 5C, MDA-MB-231 tumor xenografts accumulated greater amounts of Gd-HA than did MCF-7 tumor xenografts. Collectively, these results show that in addition to its homeostatic uptake at sites of active metabolism (e.g., the liver), detectable levels of HA probe are also taken up in tumors, which display CD44 and actively metabolize HA.

**HA Probes Target Repairing Tissues.** Both CD44 and RHAMM are most active in binding HA following tissue injury when HA is being actively metabolized. CD44 is particularly implicated in these injury-related processes.<sup>1,3,9,16,51</sup> Nevertheless, to our knowledge, the ability of HA probes to target repairing tissues has not previously been demonstrated. We assessed TR-HA uptake in two culture models that replicate aspects of vascular tissue injury in vivo. These included response to scratch-wounding and response to serum supplementation after serum starvation. Fibroblasts and smooth muscle cells were used in these experiments because both cell types contribute to vascular injury such as balloon angioplasty.<sup>59,60</sup> As we have previously reported,<sup>40</sup> scratch-wounding of fibroblast monolayers resulted in a transient increase in HA production and an elevated display of both CD44 and

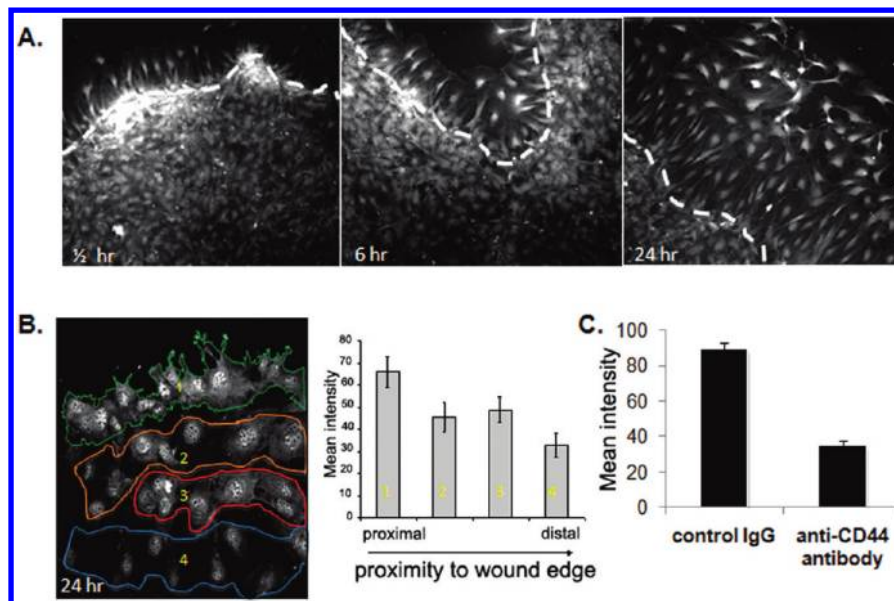


**Figure 6.** TR-HA uptake in fibroblasts increases after scratch wounding. (A) Confocal images of TR-HA uptake show that cells at the edge of wounds most strongly localize the HA probe, which is reduced with time after injury (0.5 to 24 h). (B) Fibroblasts that have migrated into the area denuded of cells continue to take up the TR-HA probe and those cells at the leading edge of the migrating population take up significantly more than those further back from the leading edge. Values shown in the histogram represent the mean and SEM ( $n = 100$  cells each in four separate experiments). (C) Uptake of TR-HA into scratch-wounded fibroblast monolayers is strongly reduced by anti-CD44 antibodies. Values represent the mean and SEM ( $n = 100$  cells in replicate experiments).

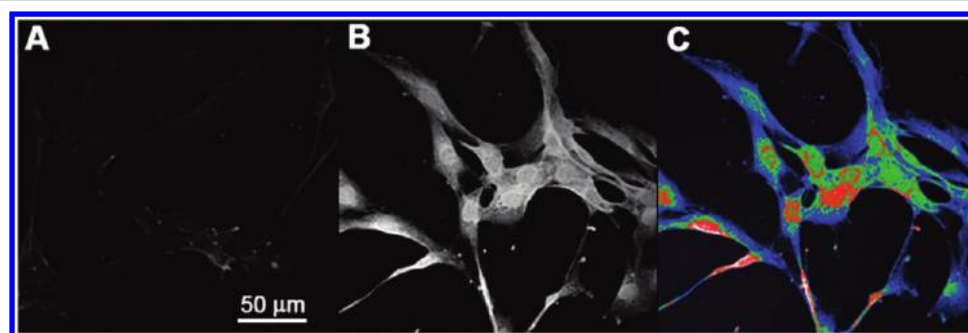


**Figure 7.** Uptake of TR-HA in smooth muscle cells following serum supplementation (serum supplementation strongly stimulates probe uptake). (A) TR-HA probe uptake in aorta smooth muscle cells serum starved for 48 h and then exposed to (B) 10% Fetal bovine serum supplements for 24 h. (C) Heat map image of B showing uptake intensity in serum supplemented cells (blue is lowest, green is intermediate and red is highest intensity).

RHAMM in the first 24–72 h<sup>40</sup> (data not shown). We quantified TR-HA uptake during the initial 24 h period following injury when cells are actively migrating in response to the scratch wound. Probe uptake at the leading edge of the monolayer increased in a linear manner between 0.25 and 2 mg/mL TR-HA probe. Fluorescence microscopy revealed that TR-HA uptake was highest at the wound edge between 0.5 and 6 h after wounding (2 mg TR-HA probe shown, Figure 6A,B). Even at 24 h, the cells located near the migratory front took up significantly more TR-HA than cells further removed from the wound edge (Figure 6A,B,  $p < 0.01$ ). Treatment with anti-CD44 Mab (Figure 6C,  $p < 0.01$ ) reduced uptake of TR-HA, indicating that probe incorporation is receptor-mediated. This temporal and spatial pattern of TR-HA uptake was closely linked to the expression of tenascin C, a marker for early stages of ECM remodeling after injury<sup>61</sup> (and data not shown).

In the second culture model, serum-starved smooth muscle cells were exposed to high levels of serum (10%) to induce a repair response. Subconfluent cells were serum-starved for 48 h, which induces quiescence then exposed to 10% serum

supplements. As shown in Figure 7, uptake of TR-HA was strongly stimulated in smooth muscle cells exposed to serum following serum starvation. Collectively, these results predict that HA probes will target injury/repair processes during early stages of ECM remodeling in vivo and that CD44 display is necessary for probe internalization.

To determine whether HA probes target to injured vascular tissue in vivo, we quantified the accumulation of either exogenous unlabeled HA or <sup>125</sup>I-HA to balloon catheter-injured arteries as a model of vessel recovery from injury or “restenosis”.<sup>62–67</sup> This procedure is designed to open occluded coronary arteries and results in increased HA metabolism and ECM remodeling.<sup>62,68</sup> In the rat, balloon catheterization also results in enhanced HA metabolism.<sup>69,70</sup> As expected, a robust acute inflammatory response<sup>71</sup> was detected shortly after balloon-induced injury (Figure 8). Accumulation of neutrophils, measured by MPO, was maximal by ~18 h postinjury (Figure 8A), whereas monocyte/macrophages influx, detected by glucosaminidase content, was maximal at 48 h after injury (Figure 8B). Balloon injury resulted in the appearance of a

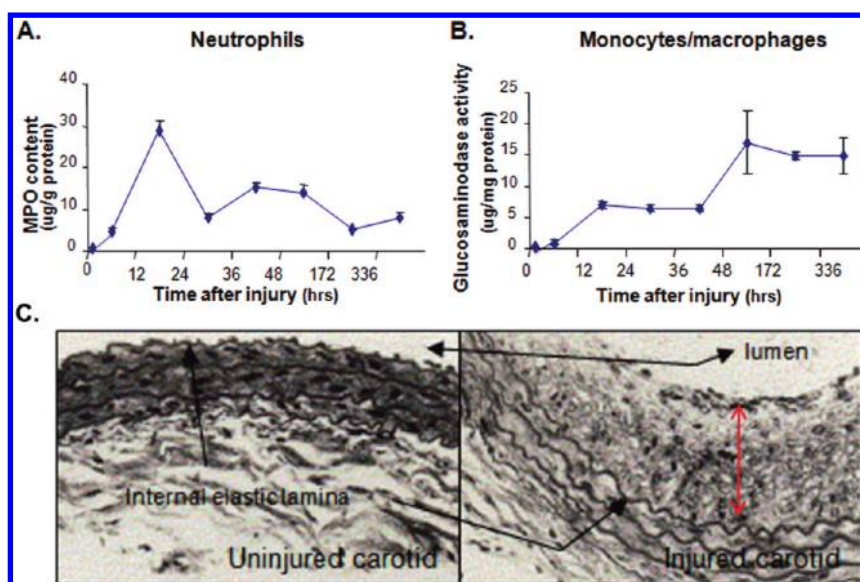


**Figure 8.** Carotid artery injury model is characterized by inflammatory cell influx and proliferation of smooth muscle cells. (A) Neutrophils, which were detected by myeloperoxidase levels, migrate into injured arteries within 24 h of balloon catheterization, after which levels progressively drop. (B) Monocyte/macrophages, detected by glucosaminidase activity, accumulate in the injured artery slightly later than neutrophils (e.g., at 48 h), and influx of these cells is sustained. (C) By 7 days after injury, a neointima is detected in the injured artery as a growth of smooth muscle cells on the luminal side of the internal elastic lamina.

neointima composed of injured smooth muscle cells that had migrated into the vessel lumen (Figure 8C), thus modeling the clinical restenosis of vessel lumen occlusion.<sup>72</sup> None of these events occurred in the contra-lateral, uninjured carotid artery (data not shown).

HA levels and RHAMM and CD44 protein expression, increased by 2 h post injury and remained high for 72 h (Figure 9 and data not shown). HA receptor expression was highest at 24 h post injury: densitometry of HA receptor expression revealed a 50% increase above basal levels at 24 h (Figure 9B). Therefore, the ability of a labeled HA probe to localize within balloon-injured arteries in vivo was assessed between 2 and 72 h post injury.

We radiolabeled tyrosine-modified HA with <sup>125</sup>I and assessed label biodistribution over 72 h following i.v. injection of 1.2–5 mg/animal (5 mg/animal shown, Table 2, Figure 10A,B). Injured and contra-lateral uninjured arteries were removed at these time points and imaged ex vivo. <sup>125</sup>I-HA accumulated in the injured but not uninjured artery between 2 and 24 h after injury (Figure 10A,B). Localization to the injured artery was reduced by coinjection of excess, unlabeled HA with the radiolabeled probe, indicating that <sup>125</sup>I-HA targeting was specific (Table 2). Furthermore, <sup>125</sup>I-CS, which does not bind to either CD44 or RHAMM,<sup>12</sup> did not localize within the injured vessel (Table 2). The reduction in probe accumulation between 2 and 24 h may be due to either probe clearance or an anti-inflammatory effect of the probe itself.<sup>18</sup> We next assessed if targeting to the injured artery was due to the HA polymer and not the result of radiolabel modification. We measured the increase in localization of HA at the site of vessel injury after i.v. injection of exogenous unlabeled HA (10 mg/kg) (Figure 10C) and compared this to buffer injection alone. A significant increase in HA accumulation was detected in injured vessels when animals were injected with unlabeled exogenous HA injected at concentrations ranging from 1 to 10 mg/kg (10 mg/kg shown, Figure 10C). These results confirm that HA conjugation to radiolabel is not responsible for its targeting

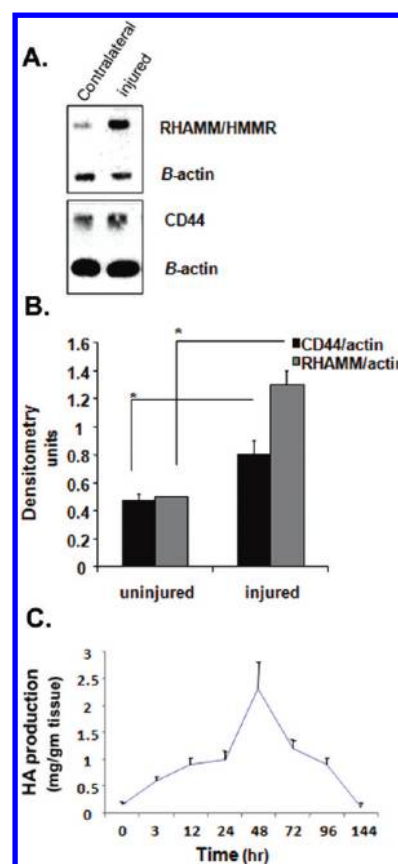


**Figure 9.** HA receptor expression increases during vascular response-to-injury. (A) Concurrent with the influx of white cells and neointima formation, protein expression of the HA receptors CD44 and RHAMM, as detected by Western blot, is increased (Student's *t* test,  $p < 0.01$ ). Values are derived from densitometry (B) and represent the mean and SEM ( $n = 3$  blots). (C) Endogenous HA accumulation in the injured vessel is transiently increased during the response-to-injury process. Values represent the mean and SEM ( $n = 4$  injured arteries).

properties and that targeting corresponds to the time in the repair process when injury-associated HA receptors are elevated.<sup>2,71</sup>

## DISCUSSION

HA plays key roles in controlling innate immune functions and fibroplasia during tissue repair following injury,<sup>17,69</sup> both of which are required for resolution of acute wounds. The extent of HA metabolism within wounds is key because it determines the quality of acute tissue repair (e.g., regenerative vs fibrotic repair).<sup>18,73</sup> Native HA promotes closure of chronic wounds such as pressure or diabetic ulcers,<sup>74,75</sup> whereas accumulation of

HA fragments promotes chronic inflammation, at least in animal models.<sup>17,76,18</sup> Despite this strong evidence linking HA to the response-to-injury process, to our best knowledge, HA-based probes have not previously been reported for imaging acute or chronically injured tissues. Our results suggest that these probes would be useful for imaging tissue healing and aid in subsequent treatment course in a number of clinical settings, for example, in tracking repair responses to such procedures as balloon angioplasty of occluded coronary arteries, healing of chronic ulcers, and repair response to stroke.

The results of the kinetic analyses in rats reported here are in agreement with our previous report in humans, which showed that HA administered by i.v. bolus (1.5–12 mg/kg) has a prolonged vascular half life.<sup>26</sup> Intriguingly, although s.c. injection of HA resulted in a lower  $C_{max}$  than i.v. injection, the half life of HA delivered s.c. is longer. This difference may be due to the release of injected HA from the skin into the circulation over an extended period. A number of reports have documented increased serum HA following administration of HA by oral gavages.<sup>32,77–79</sup> We confirmed that small but detectable increases in serum HA occurred following oral gavage of 10 mg/kg HA. However, in our study, the absorption rate was several thousand times lower than that obtained with s.c. administration of HA, and we were unable to detect targeting of <sup>125</sup>I-HA using this route of administration. Although a small amount of native HA is clearly absorbed through the gut, it is not sufficient to support use of oral HA as an imaging probe. Collectively, the absorption characteristics predict that injection of HA-based probes by either i.v. or s.c. higher at 10 mg/kg will result in serum half lives and MW sizes

**Table 2. Deposition of <sup>125</sup>I-HA and <sup>125</sup>I-CS<sup>a</sup>**

type of polymer	time after injury (h)	<sup>125</sup> I-HA or <sup>125</sup> I-CS localized (ng/mg vessel weight) <sup>b</sup>	<sup>125</sup> I-HA localized in the presence of excess unlabeled HA <sup>b</sup>
1. HA	2	20	not detected
2. HA	24	8	not detected
3. HA	48	not detected	not detected
4. HA	72	not detected	not detected
5. CS	2	not detected	NA
6. CS	24	not detected	NA

<sup>a</sup>NA=not attempted. All polymers are i.v. injected into the tail vein of rats. Amounts of deposited polymer are calculated from the known specific activity of the radiolabeled polymer described in methods and from the amount of label localized in the injured tissue. <sup>b</sup>Values are presented as the amount of <sup>125</sup>I-HA deposited in injured vessels after subtracting the amount of <sup>125</sup>I-HA localized in control, contralateral uninjured arteries.

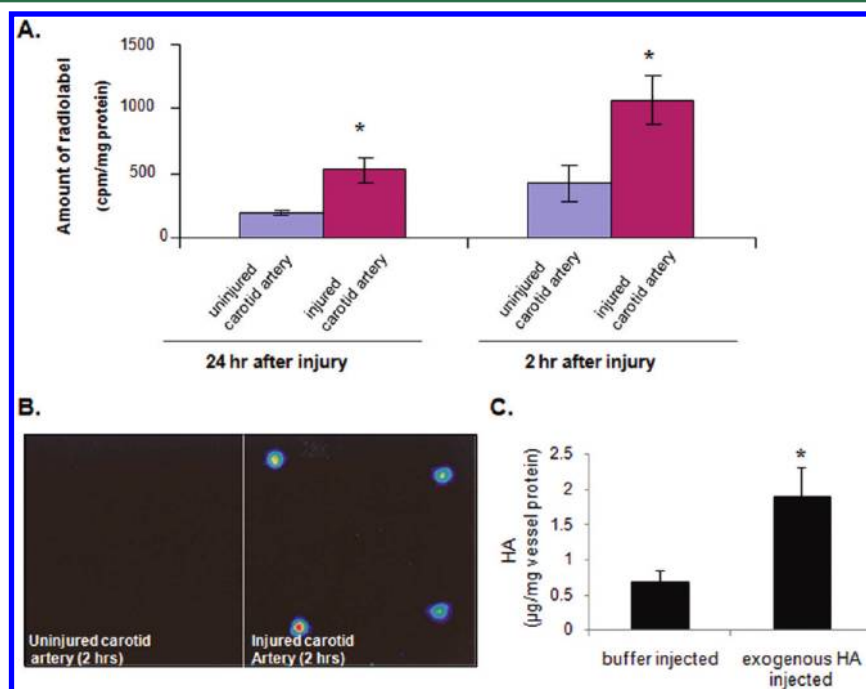


**Figure 10.** Both <sup>125</sup>I-labeled and unlabeled HA target to injured carotid arteries. (A) Localization of radiolabeled HA into injured versus uninjured contra-lateral carotid arteries after i.v. injection. The probe localized in the injured artery (\* indicates Student's *t* test,  $p < 0.01$ ) at higher levels than in the uninjured artery. Values represent the mean and SEM of data obtained from 4 animals. (B) Ex vivo Phosphor-image of injured versus uninjured arteries in panel A. Localization of probe is apparent in the injured but not the uninjured carotid artery. (C) Increased localization of HA to the injured carotid artery after i.v. administration of exogenous HA (unlabeled). Right arteries were injured, immediately injected intravenously with HA (10 mg/kg) or buffer alone, harvested 2 h later, and then analyzed for HA deposition. HA levels are significantly higher in HA-injected than buffer-injected vessels (Student's *t* test,  $p < 0.01$ ) indicating targeting of the unlabeled HA to the site of injury. Values represent the mean and SEM ( $n = 4$  animals).

that have maximal targeting properties and are suitable for imaging probe development.

We show that HA can be easily coupled to a variety of contrast agents for imaging through only minor modifications of its polymer backbone. This results in a probe that has targeting properties identical to unlabeled, exogenously supplied HA. We took advantage of different imaging modalities (i.e., nuclear, fluorescent and magnetic resonance) to obtain target-specific information in culture and in vivo. The fluorescent modality provided superb lateral resolution for quantifying specific probe uptake and localization at the cellular level (into both tumor cells and wounded cells); the MRI modality revealed anatomical details and provided sufficient depth/temporal resolution for evaluating efficacy of targeting in tumor xenografts and 3-D cultures; and the radiolabeled modality allowed sensitive monitoring of probe biodistribution and localization (i.e., ng quantities) under both homeostatic and injury conditions.<sup>72,80</sup> The TR-HA and Gd-HA uptake was significantly higher in MDA-MB-231 cell line and xenograft, which expressed high levels of CD44 than that of MCF-7, which expressed low levels of CD44.<sup>27</sup> Although HA probe uptake in culture by MDA-MB-231 BCA cells is clearly mediated by CD44, other factors in particular increased permeability of tumor,<sup>81</sup> and wound blood vessels could also have contributed to preferential probe retention at site in vivo. Our results are consistent with a key role for CD44 in the selective targeting of our HA probes, as has previously been described for HA coated liposomes.<sup>82</sup> Additional studies are required to determine if other HA receptors are also involved in probe targeting. These results also confirm and extend previous studies showing that HA-coated liposomes loaded with either gadolinium or therapeutic drugs<sup>25,82–84</sup> preferentially localize at tumor sites that express high levels of CD44 and RHAMM.

Our findings provide a molecular and functional basis for the concept of using HA as an imaging probe by itself, without a requirement for liposomal delivery. These probes may be particularly useful in detecting and spatially delineating autoimmune and chronic inflammatory diseases, which like tumors and injured tissues, share a strong inflammatory involvement. The targeting properties, combined with the nonantigenicity, excellent biocompatibility, the hydrophilic/anionic nature of HA, and its regulatory status<sup>55</sup> should permit rapid development of HA-based imaging probes. Owing to its multiple functional groups, a single HA polymer could also incorporate multiple imaging modalities, making it a promising molecule for multimodal probe design, which would meet rapidly growing needs in the clinic. Because biological processes that are imaged by probes often occur in the same sites that are targeted by therapeutics, ultimately, HA-based imaging probes can also be engineered to concomitantly deliver therapeutics with a high affinity and tissue selectivity, thus allowing real-time detection of targeting and consequences of the therapeutics on the diseased tissue.

## CONCLUSIONS

HA has previously been conjugated to nanoparticles and liposomes as a method for targeting tumors, lymphatic tissue, and liver endothelium. Here we show that HA probes also target efficiently to sites of response-to-injury, which is a process that involves higher HA metabolism and display of HA receptors such as CD44 and RHAMM. We utilized an integrated strategy that took into account the biology of target tissues and their microenvironment, the pharmacokinetics of

probes, the optimum routes of deliveries, and different imaging modalities. Our results demonstrate that native HA by itself could provide a flexible core for incorporation of multiple imaging modalities. Consistent with our hypothesis, different modalities of HA-based probes target selectively to sites of high HA receptor display in homeostatic, neoplastic, and injured tissues that have established high HA metabolism. HA probes may also be useful for studying the similarities between tissue repair and neoplasia and for designing novel, multimodal imaging, and therapeutic tools.

## AUTHOR INFORMATION

### Corresponding Author

\*E-mail: Eva.Turley@lhsc.on.ca. Tel: 519-685-8600, ext 53677. Fax: 519-685-8616.

## ACKNOWLEDGMENTS

This work was supported by a DOD-BCRP IDEA award to M.J.B. and E.A.T. (BC044087); grants from the U.S. Department of Energy, Office of Biological and Environmental Research and Low Dose Radiation Program (contract no. DE-AC02-05CH1123); by National Cancer Institute (awards R37CA064786, U54CA126552, R01CA057621, U54CA112970, U01CA143233, and U54CA143836 - Bay Area Physical Sciences—Oncology Center, University of California, Berkeley, California); and by U.S. Department of Defense (W81XWH0810736) to M.J.B.; funding from Hyal Pharma Corp. (Mississauga, ON, Canada) to E.A.T. and D.M.; National Institute of Health awards (HL075930, HL62472, HL62868) to R.S., the Ontario Institute for Cancer Research) to L.G.L., E.A.T., and T.-Y.L., and the Canadian Institutes of Health Research (MOP82720) to J.K.; and a Ruth L. Kirschstein National Research Service Award F32 postdoctoral fellowship from National Cancer Institute of National Institute of Health (FCA132491A) to M.V.

## REFERENCES

- (1) Tammi, M. I.; Day, A. J.; Turley, E. A. *J. Biol. Chem.* **2002**, *277*, 4581–4584.
- (2) Jiang, D.; Liang, J.; Noble, P. W. *Annu. Rev. Cell Dev. Biol.* **2007**, *23*, 435–461.
- (3) Slevin, M.; Krupinski, J.; Gaffney, J.; Matou, S.; West, D.; Delisser, H.; Savani, R. C.; Kumar, S. *Matrix Biol.* **2007**, *26*, 58–68.
- (4) Forte, A.; Della Corte, A.; De Feo, M.; Cerasuolo, F.; Cipollaro, M. *Cardiovasc. Res.* **2010**, *88*, 395–405.
- (5) Besler, C.; Doerries, C.; Giannotti, G.; Luscher, T. F.; Landmesser, U. *Expert Rev. Cardiovasc. Ther.* **2008**, *6*, 1071–1082.
- (6) Kriz, J.; Lalancette-Hebert, M. *Acta Neuropathol.* **2009**, *117*, 497–509.
- (7) Weigel, P. H.; Yik, J. H. *Biochim. Biophys. Acta* **2002**, *1572*, 341–363.
- (8) Cantor, J. O.; Nadkarni, P. P. *Inflammation Allergy: Drug Targets* **2006**, *5*, 257–260.
- (9) Noble, P. W.; Jiang, D. *Proc. Am. Thorac. Soc.* **2006**, *3*, 401–404.
- (10) Souza-Fernandes, A. B.; Pelosi, P.; Rocco, P. R. *Crit. Care* **2006**, *10*, 237.
- (11) Weigel, P. H.; DeAngelis, P. L. *J. Biol. Chem.* **2007**, *282*, 36777–36781.
- (12) Turley, E. A.; Noble, P. W.; Bourguignon, L. Y. *J. Biol. Chem.* **2002**, *277*, 4589–4592.
- (13) Rogers, P. A.; Donoghue, J. F.; Girling, J. E. *Placenta* **2008**, *29*, S48–S54.
- (14) Sironen, R. K.; Tammi, M.; Tammi, R.; Auvinen, P. K.; Anttila, M.; Kosma, V. M. *Exp. Cell Res.* **2011**, *317*, 383–391.

- (15) Wang, S. J.; Bourguignon, L. Y. *Am. J. Pathol.* **2011**, *178*, 956–963.
- (16) Toole, B. P.; Slomiany, M. G. *Semin. Cancer Biol.* **2008**, *18*, 244–250.
- (17) Veisoh, M.; Turley, E. A. *Integr. Biol.* **2011**, *3*, 304–315.
- (18) Jiang, D.; Liang, J.; Noble, P. W. *Physiol. Rev.* **2011**, *91*, 221–264.
- (19) Almond, A. *Cell. Mol. Life Sci.* **2007**, *64*, 1591–1596.
- (20) Tognana, E.; Borrione, A.; De Luca, C.; Pavesio, A. *Cells Tissues Organs* **2007**, *186*, 97–103.
- (21) Crouzier, T.; Szarpak, A.; Boudou, T.; Auzely-Velty, R.; Picart, C. *Small* **2010**, *6*, 651–662.
- (22) Tawfik, H. A. *Am. J. Ophthalmol.* **2010**, *150*, 757.
- (23) Esposito, E.; Menegatti, E.; Cortesi, R. *Int. J. Pharm.* **2005**, *288*, 35–49.
- (24) Kim, S. J.; Hahn, S. K.; Kim, M. J.; Kim, D. H.; Lee, Y. P. *J. Controlled Release* **2005**, *104*, 323–335.
- (25) Esposito, G.; Geninatti Crich, S.; Aime, S. *ChemMedChem* **2008**, *3*, 1858–1862.
- (26) Hamilton, S. R.; Veisoh, M.; Tolg, C.; Tirona, R.; Richardson, J.; Brown, R.; Gonzalez, M.; Vanzielegem, M.; Anderson, P.; Asculai, S.; Winnik, F.; Savani, R. C.; Freeman, D.; Luyt, L. G.; Koropatnick, J.; Turley, E. A. *Open Drug Metab. J.* **2009**, *3*, 43–55.
- (27) Hamilton, S. R.; Fard, S. F.; Paiwand, F. F.; Tolg, C.; Veisoh, M.; Wang, C.; McCarthy, J. B.; Bissell, M. J.; Koropatnick, J.; Turley, E. A. *J. Biol. Chem.* **2007**, *282*, 16667–16680.
- (28) Ripellino, J. A.; Klinger, M. M.; Margolis, R. U.; Margolis, R. K. *J. Histochem. Cytochem.* **1985**, *33*, 1060–1066.
- (29) Pitsillides, A. A.; Worrall, J. G.; Wilkinson, L. S.; Bayliss, M. T.; Edwards, J. C. *Br. J. Rheumatol.* **1994**, *33*, 5–10.
- (30) Yanagishita, M.; Podyma-Inoue, K. A.; Yokoyama, M. *Glycoconjugate J.* **2009**, *26*, 953–959.
- (31) Bower, L.; Braven, J.; Manley, G. *J. Pharm. Biomed. Anal.* **1988**, *6*, 67–74.
- (32) Balogh, L.; Polyak, A.; Mathe, D.; Kiraly, R.; Thuroczy, J.; Terez, M.; Janoki, G.; Ting, Y.; Bucci, L. R.; Schauss, A. G. *J. Agric. Food Chem.* **2008**, *56*, 10582–10593.
- (33) Gustafson, S.; Bjorkman, T.; Westlin, J. E. *Glycoconjugate J.* **1994**, *11*, 608–613.
- (34) Gouin, S.; Winnik, F. M. *Bioconjugate Chem.* **2001**, *12*, 372–377.
- (35) Zhu, W.; Artemov, D. *Contrast Media Mol. Imaging* **2011**, *6*, 61–68.
- (36) Shiftan, L.; Israely, T.; Cohen, M.; Frydman, V.; Dafni, H.; Stern, R.; Neeman, M. *Cancer Res.* **2005**, *65*, 10316–10323.
- (37) Underhill, C. B.; Toole, B. P. *J. Biol. Chem.* **1980**, *255*, 4544–4549.
- (38) McGuire, P. G.; Castellet, J. J. Jr.; Orkin, R. W. *J. Cell Physiol.* **1987**, *133*, 267–276.
- (39) Majack, R. A.; Clowes, A. W. *J. Cell Physiol.* **1984**, *118*, 253–256.
- (40) Savani, R. C.; Wang, C.; Yang, B.; Zhang, S.; Kinsella, M. G.; Wight, T. N.; Stern, R.; Nance, D. M.; Turley, E. A. *J. Clin. Invest.* **1995**, *95*, 1158–1168.
- (41) Silverman-Gavrila, R.; Silverman-Gavrila, L.; Hou, G.; Zhang, M.; Charlton, M.; Bendeck, M. P. *Am. J. Pathol.* **2011**, *178*, 895–910.
- (42) Nitta, T.; Okumura, K.; Sato, K. *Pathobiology* **1992**, *60*, 42–44.
- (43) Banzato, A.; Rondina, M.; Melendez-Alafort, L.; Zangoni, E.; Nadali, A.; Renier, D.; Moschini, G.; Mazzi, U.; Zanollo, P.; Rosato, A. *Nucl. Med. Biol.* **2009**, *36*, 525–533.
- (44) Dekel, Y.; Glucksam, Y.; Margalit, R. *J. Controlled Release* **2010**, *143*, 128–135.
- (45) Asari, A.; Kanemitsu, T.; Kurihara, H. *J. Biol. Chem.* **2010**, *285*, 24751–24758.
- (46) Carmona, J. U.; Arguelles, D.; Deulofeu, R.; Martinez-Puig, D.; Prades, M. *Vet. Comp. Orthop. Traumatol.* **2009**, *22*, 455–459.
- (47) Jonsson, G.; Staaf, J.; Olsson, E.; Heidenblad, M.; Vallon-Christersson, J.; Osoegawa, K.; de Jong, P.; Oredsson, S.; Ringner, M.; Hoglund, M.; Borg, A. *Genes, Chromosomes Cancer* **2007**, *46*, 543–558.
- (48) McCourt, P. A. *Matrix Biol.* **1999**, *18*, 427–432.
- (49) Gustafson, S. *Glycobiology* **1997**, *7*, 1209–1214.
- (50) Mahteme, H.; Graf, W.; Larsson, B. S.; Gustafson, S. *Glycoconjugate J.* **1998**, *15*, 935–939.
- (51) Tammi, R. H.; Kultti, A.; Kosma, V. M.; Pirinen, R.; Auvinen, P.; Tammi, M. I. *Semin. Cancer Biol.* **2008**, *18*, 288–295.
- (52) Prevo, R.; Banerji, S.; Ni, J.; Jackson, D. G. *J. Biol. Chem.* **2004**, *279*, 52580–52592.
- (53) Prestwich, G. D.; Kuo, J. W. *Curr. Pharm. Biotechnol.* **2008**, *9*, 242–245.
- (54) Baldwin, A. D.; Kiick, K. L. *Biopolymers* **2010**, *94*, 128–140.
- (55) Burdick, J. A.; Prestwich, G. D. *Adv. Mater.* **2011**, *23*, H41–H56.
- (56) Noel, A.; Borcy, V.; Bracke, M.; Gilles, C.; Bernard, J.; Birembaut, P.; Mareel, M.; Foidart, J. M. *Anticancer Res.* **1995**, *15*, 1–7.
- (57) Wang, F.; Hansen, R. K.; Radisky, D.; Yoneda, T.; Barcellos-Hoff, M. H.; Petersen, O. W.; Turley, E. A.; Bissell, M. J. *J. Natl. Cancer Inst.* **2002**, *94*, 1494–1503.
- (58) Slomiany, M. G.; Dai, L.; Tolliver, L. B.; Grass, G. D.; Zeng, Y.; Toole, B. P. *Clin. Cancer Res.* **2009**, *15*, 7593–7601.
- (59) Wilcox, J. N.; Okamoto, E. I.; Nakahara, K. I.; Vinten-Johansen, J. *Ann. N.Y. Acad. Sci.* **2001**, *947*, 68–90; discussion 90–92.
- (60) Stenmark, K. R.; Bouchev, D.; Nemenoff, R.; Dempsey, E. C.; Das, M. *Physiol. Res.* **2000**, *49*, 503–517.
- (61) Tolg, C.; Hamilton, S. R.; Nakrieko, K. A.; Kooshesh, F.; Walton, P.; McCarthy, J. B.; Bissell, M. J.; Turley, E. A. *J. Cell Biol.* **2006**, *175*, 1017–1028.
- (62) Savani, R. C.; Turley, E. A. *Int. J. Tissue React.* **1995**, *17*, 141–151.
- (63) Heublein, B.; Evagorou, E. G.; Rohde, R.; Ohse, S.; Meliss, R. R.; Barlach, S.; Haverich, A. *Int. J. Artif. Organs* **2002**, *25*, 1166–1173.
- (64) Chajara, A.; Raoudi, M.; Delpech, B.; Levesque, H. *Atherosclerosis* **2003**, *171*, 15–19.
- (65) Thierry, B.; Winnik, F. M.; Merhi, Y.; Silver, J.; Tabrizian, M. *Biomaterials* **2004**, *25*, 3895–3905.
- (66) Stewart, H. J.; Guildford, A. L.; Lawrence-Watt, D. J.; Santin, M. *J. Biomed. Mater. Res., Part A* **2009**, *90*, 465–471.
- (67) Kim, T. G.; Lee, H.; Jang, Y.; Park, T. G. *Biomacromolecules* **2009**, *10*, 1532–1539.
- (68) Savani, R. C.; Cao, G.; Pooler, P. M.; Zaman, A.; Zhou, Z.; DeLisser, H. M. *J. Biol. Chem.* **2001**, *276*, 36770–36778.
- (69) Wight, T. N. *Front. Biosci.* **2008**, *13*, 4933–4937.
- (70) Savani, R. C.; Khalil, N.; Turley, E. A. *Proc. West. Pharmacol. Soc.* **1995**, *38*, 131–136.
- (71) Shirali, A. C.; Goldstein, D. R. *Curr. Opin. Organ Transplant* **2008**, *13*, 20–25.
- (72) Werner, G. S.; Gitt, A. K.; Zeymer, U.; Juenger, C.; Towae, F.; Wienberger, H.; Senges, J. *Clin. Res. Cardiol.* **2009**, *98*, 435–441.
- (73) Gurtner, G. C.; Werner, S.; Barrandon, Y.; Longaker, M. T. *Nature* **2008**, *453*, 314–321.
- (74) Weindl, G.; Schaller, M.; Schafer-Korting, M.; Korting, H. C. *Skin Pharmacol. Physiol.* **2004**, *17*, 207–213.
- (75) Abbruzzese, L.; Rizzo, L.; Fanelli, G.; Tedeschi, A.; Scatena, A.; Goretti, C.; Macchiarini, S.; Piaggini, A. *Int. J. Lower Extremity Wounds* **2009**, *8*, 134–140.
- (76) Namazi, M. R.; Fallahzadeh, M. K.; Schwartz, R. A. *Int. J. Dermatol.* **2011**, *50*, 85–93.
- (77) Bergin, B. J.; Pierce, S. W.; Bramlage, L. R.; Stromberg, A. *Equine Vet. J.* **2006**, *38*, 375–378.
- (78) Huang, S. L.; Ling, P. X.; Zhang, T. M. *World J. Gastroenterol.* **2007**, *13*, 945–949.
- (79) Piao, M. G.; Kim, J. H.; Kim, J. O.; Lyoo, W. S.; Lee, M. H.; Yong, C. S.; Choi, H. G. *Drug Dev. Ind. Pharm.* **2007**, *33*, 485–491.
- (80) Benaron, D. A. *Cancer Metastasis Rev.* **2002**, *21*, 45–78.
- (81) Cheong, S. J.; Lee, C. M.; Kim, E. M.; Uhm, T. B.; Jeong, H. J.; Kim, D. W.; Lim, S. T.; Sohn, M. H. *Nucl. Med. Biol.* **2011**, *38*, 93–101.
- (82) Qhattal, H. S.; Liu, X. *Mol. Pharm.* **2011**, *8*, 1233–1246.
- (83) Toriyabe, N.; Hayashi, Y.; Hyodo, M.; Harashima, H. *Biol. Pharm. Bull.* **2011**, *34*, 1084–1089.
- (84) Surace, C.; Arpicco, S.; Dufay-Wojcicki, A.; Marsaud, V.; Bouclier, C.; Clay, D.; Cattel, L.; Renoir, J. M.; Fattal, E. *Mol. Pharm.* **2009**, *6*, 1062–1073.